Tuning in to star-planet interactions at radio wavelengths

Kavanagh, R.D.

1 | Introduction

1.1 The discovery of the solar wind

The first suggestion that the Sun, our closest star, is a source of outflowing hot magnetised plasma came from the Norwegian physicist Kristian Birkeland in the early 1900s, who illustrated a striking similarity between the results of his experiments firing beams of electrons at a spherical magnet and the Northern Lights (Birkeland, 1908). This idea was further reinforced by Biermann (1951), who proposed that the formation of Type I tails from comets could be explained by outflowing ionised plasma from the Sun at supersonic speeds of $\sim$ 1000 km s^{-1}, which we now know as the *solar wind*. In the meantime, evidence began to mount supporting the existence of the solar corona shown in Figure 1.1, the million degree Kelvin (K) region of the Sun's upper atmosphere (Grotrian, 1939; Alfvén, 1941; Edlén, 1945). It was Parker (1958) who first linked the idea of a hot corona to a continuously outflowing solar wind in a self-consistent way.

Parker's approach was simple but very effective. He described the solar wind as being driven by a strong thermal pressure gradient set by the hot corona, offset by the gravitational pull of the Sun. By assuming that the solar wind is isothermal (i.e. the temperature does not change with distance), maintains a negative pressure gradient, and is an ideal gas, Parker derived a differential equation describing the momentum of the solar wind outflow. While Parker found that there were a family of solutions to this equation, only one described a solar wind outflow that monotonically increased in velocity outwards, transitioning from a subsonic regime to a supersonic regime. This was in agreement with the likes of Biermann (1951), who suggested the same scenario for a supersonic solar wind outflow.

While Parker's solar wind solution was initially met with strong criticism, measurements obtained by the Mariner 2 spacecraft in 1962 quickly put to rest any doubts about its existence (Neugebauer & Snyder, 1966). At 1 au, Mariner 2 detected a solar wind outflow with a supersonic velocity of 500 km s^{-1} and a proton density of 5 cm^{-3} on average. Integrating the mass flux over 4π steradians, the solar wind mass-loss rate measured by Mariner 2 was $\sim 6 \times 10^{11}$ g s^{-1}, in close agreement with the now-accepted value of 2×10^{-14} $M_\odot$ yr^{-1} (Feldman et al., 1977; Cohen, 2011; Finley et al., 2019). Parker's solar wind solution for a coronal temperature of 1 MK and mass-loss rate of 2×10^{-14} $M_\odot$ yr^{-1} gives values that are in fantastic agreement with those obtained by Mariner 2 at 1 au, with a predicted velocity and density of 485 km s^{-1} and 5.5 cm^{-3} respectively. The velocity

and density profile obtained using his prescription is shown in Figure 1.2.

Our understanding of the solar wind has advanced significantly since the 1960s, thanks to a multitude of in-situ measurements (Verscharen et al., 2019) and ever-more sophisticated modelling (for a review, see Gombosi et al., 2018). In terms of modelling, the most significant improvements have been the inclusion of rotation and magnetic fields, aspects which were lacking in the initial model of Parker (1958). While Parker (1958) commented on the likely morphology of the large-scale solar magnetic field (the Parker spiral), it was Weber & Davis (1967) who first provided a solar wind model which accounted for these effects in a self-consistent way. Weber & Davis (1967) illustrated that the Sun loses angular momentum, both through the solar wind outflow, as well as via the torque of the large-scale field magnetic field acting on the wind. Understanding the angular momentum loss-rate of the Sun tells us how it will spin down over time (Gallet & Bouvier, 2013; Ó Fionnagáin & Vidotto, 2018; Vidotto, 2021).

The Sun is magnetised at its surface, and therefore any fluid prescription for the solar wind outflow is governed by magnetohydrodynamics (MHD). Its magnetic field is also not a perfect dipole, but contains fine structure and non-uniformities, requiring a 3-dimensional analysis. Another main improvement to theoretical understanding of the solar wind outflow is a prescription for the energy that drives it. Known as the 'coronal heating problem', it is an outlying problem in plasma physics as to what ultimately heats the solar corona to a million degrees K. A widely-accepted solution to this problem is that the energy source is the dissipation of Alfvén waves, which are mechanical waves that travel along magnetic field lines (Alfvén, 1942). Observations of Alfvén waves in the upper regions of the Sun's atmosphere seem to support this hypothesis (De Pontieu et al., 2007; McIntosh et al., 2011). Following this, a 3D MHD solar wind model was developed that is driven by the dissipation of Alfvén waves, known as the AWsom Solar Model (AWSoM, Sokolov et al., 2013; van der Holst et al., 2014). AWSoM has been used to successfully reproduce images of the solar corona in extreme UV (EUV), as shown in Figure 1.3.

1.2 Interactions between the solar wind and the planets

With the discovery of the solar wind, we soon began to understand its interactions and effects on the solar system planets. The most well-known example on Earth is the Northern/Southern lights, also known as the aurora borealis/australis, or more generally, aurorae (shown in Figure 1.4). From as early as the 1700s, it was understood that their appearance in the night sky generally followed the phenomenon of so-called 'magnetic storms', which were thought to be some kind of perturbation of the Earth's magnetic field (Stern, 1989). We now understand their formation on Earth as a result of the Dungey cycle (Dungey, 1961), which describes how the magnetic field carried by the solar wind compresses the nightside of the Earth's magnetic field (also known as the magnetotail), causing magnetic reconnection to occur. A sketch of this process is shown in Figure 1.5.

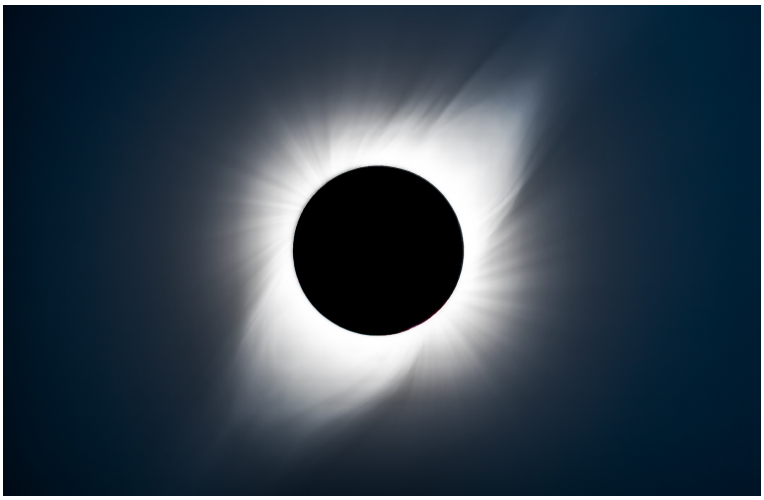

Figure 1.1: Image of the Sun's corona taken during the total solar eclipse on July 2nd 2019 near La Silla observatory in Chile. The dipolar structure of the Sun's magnetic field threading the coronal plasma can be seen clearly. Image credit: Joe Llama.

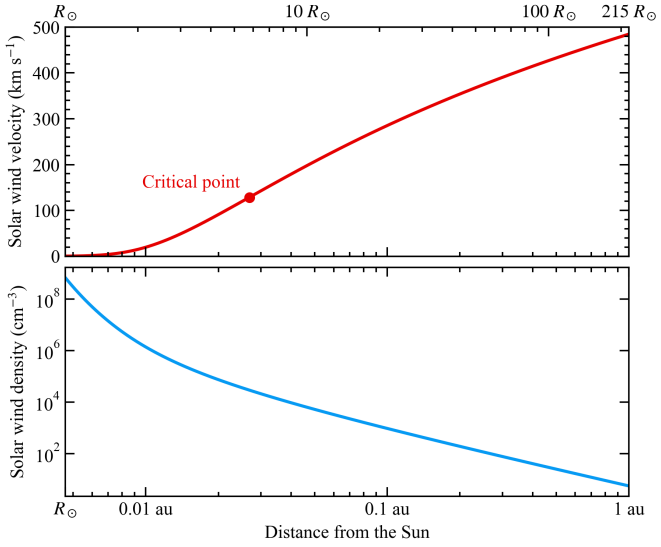

Figure 1.2: *Top*: Velocity profile of the solar wind from the solar surface to 1 au $\equiv 215\ R_\odot$ (the orbital distance of Earth), obtained using the solution from Parker (1958) for a temperature of 1 MK (numerical code developed by Kavanagh & Vidotto, 2020). The critical point, where the solar wind becomes supersonic, is marked. *Bottom*: Density profile of the solar wind for a mass-loss rate of 1.261×10^{12} g s^{-1}.

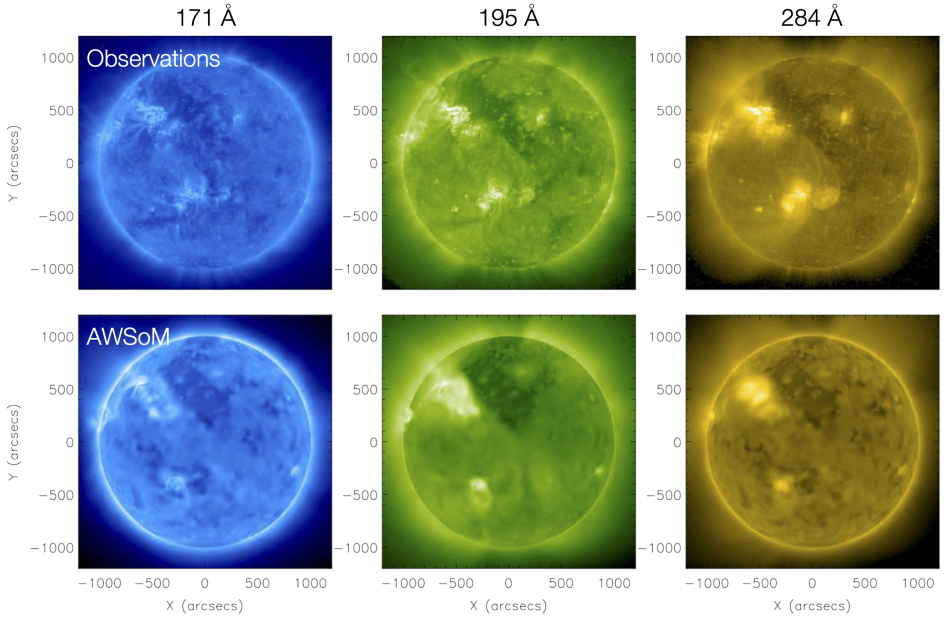

Figure 1.3: Comparison of the solar corona imaged at 3 EUV wavelengths with the STEREO-A satellite on March 11th 2007 (top panels) to those produced with the Alfvén wave-driven solar wind model AWSoM (bottom panels). Figure adapted from van der Holst et al. (2014).

Figure 1.4: The Earth's aurora as seen from the surface over Adventdalen, Svalbard, at a latitude of 78.2 degrees North. The distinct green colour is clearly visible, which is formed via state transitions in oxygen that occur due to the collision of electrons accelerated in the Earth's magnetotail with the atmosphere (He et al., 2020). Image by Sean Coney.

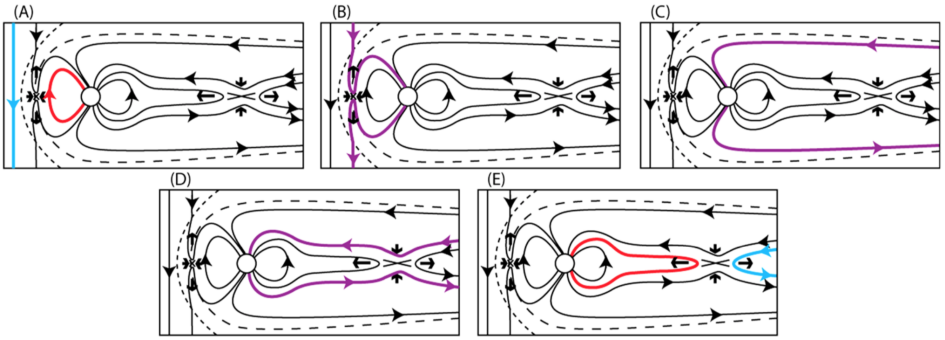

Figure 1.5: Sketch depicting the formation mechanism for the aurorae on Earth proposed by Dungey (1961). Panel A depicts the solar wind magnetic field (blue) interacting with and opening the Earth's magnetic field at the nose of its magnetopause (red). In panels B to D, the two components of this now-open field line (purple) are pushed back towards the magnetotail in the Earth's magnetosphere (right-hand side of each panel). Finally, these two lines reconnect in the magnetotail, releasing energy which accelerates electrons towards the Earth's magnetic pole (red) and into the plasma sheet (blue). The injection of these high-velocity electrons into the Earth's polar regions is thought to be the main driver of the aurorae. Figure from Eastwood et al. (2015).

The energy released during reconnection events in the Earth's magnetotail accelerates electrons towards the magnetic poles of the Earth, resulting in emission across the electromagnetic spectrum. These electrons collide with atoms and molecules in the Earth's upper atmosphere, producing visible light with the distinct red, green, and blue colours that are commonly associated with the aurorae (He et al., 2020), as well as at infrared wavelengths (Espy et al., 1988). Higher energy emission at UV (Paresce, 1979) and X-ray wavelengths (Bhardwaj et al., 2007) is also generated in the Earth's auroral zones, via charge exchange and thermal emission processes respectively. At lower frequencies, the introduction of high-velocity electrons into the polar regions is thought to produce kHz radio emission via the electron cyclotron maser instability (Lamy et al., 2010), which generates 100% circularly polarised radio emission (Dulk, 1985).

Aurorae are not limited to the Earth's magnetic field. In fact, they are ubiquitous in the magnetic polar regions of all the magnetised solar system planets (Mercury, Earth, Jupiter, Saturn, Uranus, and Neptune). It was not until the Voyager spacecraft ventured out into the solar system however that we first learned of their existence on the giant planets, primarily at radio and UV wavelengths (Zarka, 1998; Grodent, 2015). Mercury on the other hand has not been found to exhibit aurorae, primarily due to its lack of an atmosphere (Saur et al., 2021). In Figure 1.6, I show a comparison of the experiments performed by Kristian Birkeland in the early 1900s to Jupiter's aurora imaged in the UV by the Hubble Space Telescope.

Subsequent observations have found that the aurorae of the other magnetised solar system planets appear across the electromagnetic spectrum in a same manner to Earth (Badman et al., 2015). For Jupiter and Saturn, dedicated missions

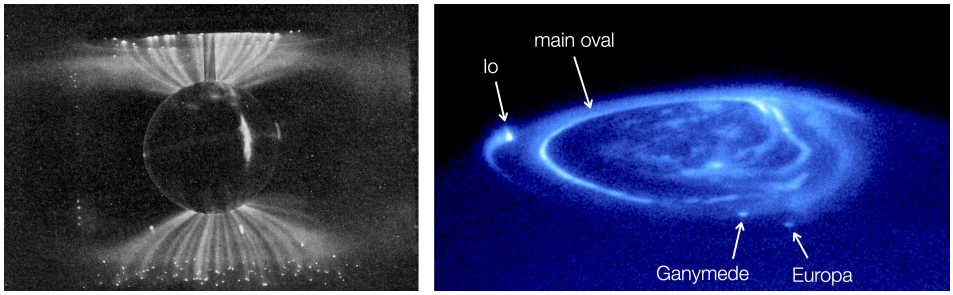

Figure 1.6: *Left*: Photograph of Kristian Birkeland's 'terrella' experiment, wherein he fired an electron beam at a spherical magnet inside a vacuum chamber to investigate the formation of the aurora on Earth. Note the formation of bright rings near the magnetic poles (from Birkeland, 1908). *Right*: UV image of the aurora at Jupiter's North pole, taken with the Hubble Space Telescope (NASA/ESA, John Clarke). The main auroral oval is indicated, along with the footpoints of the field lines of Jupiter connecting to the moons Io, Ganymede, and Europa. The footpoint of Callisto is thought to be obscured by the main auroral oval (Saur et al., 2013).

such as Galileo, Juno, and Cassini have revealed the complexities relating to the formation of their aurorae (see Grodent, 2015; Stallard et al., 2019; Bonfond et al., 2020; Zarka et al., 2021). For Uranus and Neptune however, our understanding of their aurorae is currently limited to the data obtained by the Voyager satellites (Lamy, 2020). Irrespective of these technicalities, the auroral emission of the magnetised planets at radio wavelengths seems to be controlled by the solar wind power incident on their magnetospheres (Desch & Kaiser, 1984; Zarka, 2007). This relation is known as the 'radiometric Bode's law', which is shown in Figure 1.7. At low frequencies (< 100 MHz), Jupiter's auroral emission outshines the Sun by over three orders of magnitude (Zarka, 2007).

Although not directly linked to interactions with the solar wind, prominent features in Jupiter's aurora are bright spots associated with the magnetic field lines linking the planet to its moons Io, Europa, and Ganymede, as shown in the right panel of Figure 1.6. These are thought to be powered by sub-Alfvénic interactions between the moons and Jupiter, which perturb the Jovian magnetic field and produce Alfvén waves (Neubauer, 1980). These waves carry energy back towards Jupiter, which is subsequently dissipated at various different wavelengths, again most notably in the UV and radio (Zarka, 2007). An interesting note is that the radio component of the Jupiter-Io sub-Alfvénic interaction was identified as early as the 1960s by Bigg (1964), who noted that bright radio emission originating from Jupiter was coincident with the quadratures of Io (where the maximum angular separation occurs between the two bodies from our perspective). More recently, moon-induced emission from Enceladus has also been identified on Saturn in the UV (Pryor et al., 2011).

In the context of the weakly/unmagnetised solar system planets like Venus and Mars, interactions with the solar wind are also important for their atmospheric evolution. It is likely that at earlier ages, the solar wind was much stronger

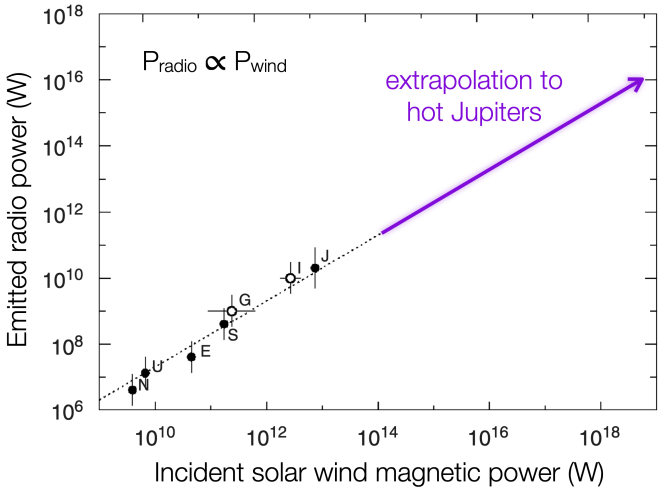

Figure 1.7: The empirically-derived radiometric Bode's law for the magnetised solar system planets, namely Earth (E), Jupiter (J), Saturn (S), Uranus (U), and Neptune (N). The power dissipated onto Jupiter from sub-Alfvénic interactions with its moons Io (I) and Ganymede (G) are also shown, which appears to follow the same trend. The power law relation between the incident solar wind and the emitted radio emission is linear, with an efficiency ratio of $\sim 2 \times 10^{-3}$. The extrapolation of this relation to the likely stellar wind environments of hot Jupiters is also shown. I will discuss this further in Section 1.5. Figure adapted from Zarka (2007).

compared to the present-day (Ó Fionnagáin & Vidotto, 2018). As a result, these two planets were likely to have been subjected to much harsher conditions. Due to the lack of intrinsic magnetic fields, the solar wind can remove a significant amount of material from their upper atmosphere (Kulikov et al., 2007; Curry et al., 2015). Combined with the harsher conditions at earlier ages, the removal of material from the atmospheres of Venus and Mars by the solar wind was likely to be even more significant.

1.3 The stellar wind environments around exoplanets

Wind outflows are not unique to the Sun. In fact, evidence for winds emanating from other stars came prior to Parker (1958) via spectroscopic features, from the likes of Beals (1929), Kosirev (1934), and Deutsch (1956), albeit for stars more massive/evolved than the Sun. Following from Parker's prescription for the solar wind, these signatures of outflowing material from other stars were re-interpreted as stellar winds, which are now evident across the HR diagram (Deutsch, 1969). Their existence also alleviated issues relating to how stars evolve towards the ends of their lives (e.g. Cameron, 1959; Parker, 1960).

An important thing to note is that all the stars identified to be undergoing mass-loss via stellar winds prior to the late 90s were massive/evolved stars (apart from the Sun). The winds of these stars are distinct from the solar wind, in that they are thought to be driven by momentum transfer from the stellar radiation field, via either absorption from dust grains or scattering from the opacity of ions (Lamers & Cassinelli, 1999). These are often referred to as *dust/continuum*-driven and *line/radiatively*-driven winds respectively. This bias towards their earlier detection is due to the fact that their mass-loss rates are many orders of magnitude greater than the solar wind, and therefore have denser and faster winds which can produce strong spectral signatures. These spectroscopic features that are powerful diagnostics tools for the winds of massive and evolved stars are known as P Cygni profiles (see Puls et al., 2008).

While it was the winds of massive/evolved stars that were initially discovered, these are not representative of the majority of stars in our galaxy. The primary stellar components of the galaxy are *low-mass* stars on the main-sequence, which are powered by burning hydrogen in their cores. These stars are of spectral types M, K, G, or F, and have masses ranging from around 0.1 to 1.5 solar masses ($M_{\odot}$), and effective temperatures from 2400 to 7200 K[1]. Within 10 parsecs of the solar system, low-mass stars comprise 93% of all stars, with M dwarfs being the most numerous at 75% (see RECONS, the REsearch Consortium On Nearby Stars).

Like the Sun, low-mass main-sequence stars exhibit hot coronae, as is evident from their prominent X-ray emission (Güdel, 2004; **?**). They also possess surface magnetic fields, which are thought to be generated and sustained by convective dynamos (Christensen et al., 2009). The magnetic fields of M dwarfs can be

[1] A Modern Mean Dwarf Stellar Color and Effective Temperature Sequence

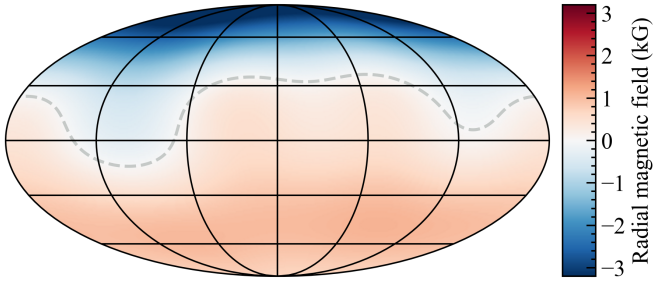

Figure 1.8: The radial surface magnetic field of the active M dwarf WX UMa. Maps such as this are reconstructed from spectropolarimetric observations, using the method known as Zeeman-Doppler imaging (ZDI, Semel, 1989). The field here is well-described by a dipole that is aligned with the rotation axis of the star, with a maximum strength of 3 kilogauss. Figure from Kavanagh et al. (2022) based on Morin et al. (2010).

upwards of a kilogauss in strength (Morin et al., 2010), three orders of magnitude higher than the present-day Sun (see Figure 1.8). There is a strong relationship that holds over many orders of magnitude between the inferred surface magnetic fluxes of low-mass stars and their X-ray emission, implying that their coronae are magnetically heated (see Figure 1.9; Pevtsov et al., 2003; Vidotto et al., 2014). Coronal X-rays have been identified on stars as massive as A7V ($\sim$ 1.7 $M_{\odot}$, Schmitt et al., 1985; Peterson et al., 2006). Above this mass threshold, stars are thought to transition to having radiative outer envelopes, lacking convection and therefore the ability to sustain a dynamo-driven magnetic field. The evidence for hot, magnetically-active coronae on low-mass main-sequence stars naturally suggests that they are sources of solar-like *coronal* winds.

Low-mass main sequence stars are not only likely to have coronal winds, but they also are found to host the bulk of the 5000+ exoplanets discovered to date. As these stars can remain on the main-sequence for billions of years, understanding their stellar wind environments is crucial to determining the long-term effects of the wind outflows on the orbiting planets. M dwarfs are of particular interest in this context, as they are both the most numerous in the galaxy, and are expected to host the majority of Earth-like planets (see Gaidos et al., 2016; Burn et al., 2021). This is not currently reflected in exoplanet statistics however, as M dwarfs can exhibit high levels of activity which can hinder the detection of orbiting Earth-like planets through traditional methods (e.g. Lanza et al., 2011; Andersen & Korhonen, 2015). In Figure 1.10, I show the breakdown of the number of exoplanets found to orbit main-sequence stars as a function of their spectral type.

1.4 Measuring the winds of low-mass stars

The first evidence of winds originating from low-mass stars was presented by Wood et al. (1996). Based on density maps of the local interstellar medium (ISM),

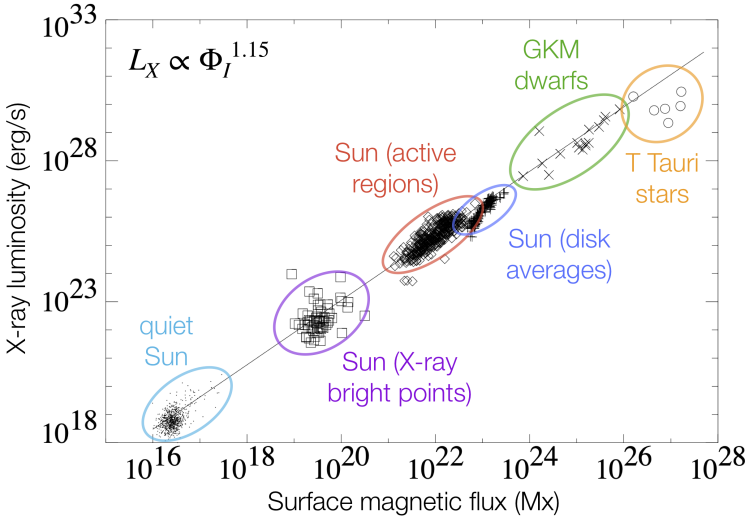

Figure 1.9: The observed relationship between the surface magnetic flux of low-mass stars and their X-ray emission. The data are from the Sun, main-sequence G, K, and M dwarfs, and pre-main-sequence T Tauri stars. A power-law fit to the data indicates that the X-ray luminosity L_X is proportional to the magnetic flux ${\Phi_I}^{1.15}$, implying that their X-ray emission is produced via magnetic heating in their coronae. Note that the magnetic flux values here are derived from the Zeeman broadening method, which are typically denoted with the subscript 'I', whereas those derived from maps obtained via the ZDI method (i.e. Figure 1.8) are denoted with the subscript 'V' (see Kochukhov, 2021). Figure adapted from Pevtsov et al. (2003).

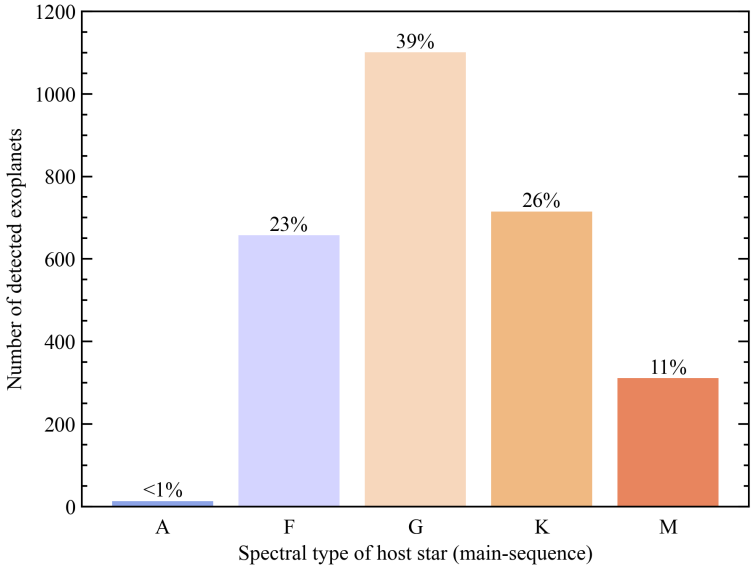

Figure 1.10: The number of exoplanets detected to orbit main-sequence stars as a function of the host star spectral type. The vast majority of exoplanet discovered to date are found to orbit main-sequence F–M stars, which are expected to exhibit coronal, solar-like stellar winds. The percentage of exoplanets detected orbiting main-sequence stars of each spectral type are shown above each bar. Data taken from the NASA Exoplanet Archive on June 14th 2022. Note that many of the host stars in the database used here do not have catalogued spectral types, so I have identified them using their effective temperatures and radii based on "A Modern Mean Dwarf Stellar Color and Effective Temperature Sequence".

observations with the Hubble Space Telescope revealed that Lyman α emission from some stars was absorbed to a greater extent than what was expected from purely the ISM. At the same time, theoretical models had been proposed which predicted the existence of a 'wall' of hot neutral hydrogen at the heliopause (Pauls et al., 1995), the region where there is pressure balance between the ISM and solar wind outflow. This is effectively a scaled-up version of a planetary magnetopause. This wall of neutral hydrogen is thought to form due to the compression and heating of the ISM due to the motion of the heliosphere, the region inside the heliopause, through the ISM (Wood et al., 2021).

While the excess absorption of Lyman α emission from some stars could be attributed to a neutral hydrogen wall at the Sun's heliopause, Wood et al. (1996) found that it was still not sufficient to explain the Lyman α profiles from the stars ϵ Eri and λ And. Wood et al. (1996) therefore proposed that walls of neutral hydrogen could exist around these stars also at their astropauses, the stellar equivalent of a heliopause, formed in a similar manner as what was proposed for the Sun. The scenario suggested by Wood et al. (1996) is described in Figure 1.11. The implication that these stars had heliospheres of their own, called astrospheres, meant that they also had winds. This fit the narrative of these stars possessing coronae, which had been suggested based on X-ray observations of main-sequence stars up to spectral types of A7 (Schmitt et al., 1985). With a hot coronae, these stars could drive a thermally-expanding stellar wind outflow in the same manner as proposed by Parker (1958) for the Sun.

Since the initial proposal of Wood et al. (1996), around 30 main-sequence stars have been identified to exhibit Lyman α absorption profiles consistent with that expected from hydrogen walls at their astropauses (Wood et al., 2021). Using hydrodynamical models of stellar astrospheres, the Lyman α profiles of these stars have been fit to determine their mass-loss rates. To date, this has been the most successful method for measuring the winds of low-mass stars (Vidotto, 2021). More recently however, other methods have also been used successfully to estimate stellar wind mass-loss rates, namely based on the presence of prominences around the star (Jardine & Collier Cameron, 2019), and the evaporation of exoplanetary atmospheres (Vidotto & Bourrier, 2017). Additionally, non-detections of thermal radio emission from the winds of low-mass main-sequence stars can provide useful upper-limits for their mass-loss rates (e.g. Fichtinger et al., 2017).

In Figure 1.12, I show the inferred mass-loss rate per unit surface area for low-mass main-sequence stars as a function of their surface X-ray fluxes. A power-law fit to the data indicates a relationship between the two quantities, implying that the energy source powering their X-ray emission also drives the wind outflows from the coronae of these stars. This power law can be used to link the mass-loss rates of low-mass main-sequence stars to their magnetic field strengths. Figure 1.9 shows the relation between the X-ray luminosity and surface magnetic fluxes derived using the Zeeman broadening method (Φ_I). However, a large fraction of the stars shown in Figure 1.12 have reconstructed surface magnetic field maps available, such as that shown in Figure 1.8 (see Morin et al., 2008a; Vidotto et al., 2014, 2016; Folsom et al., 2018; See et al., 2019; Klein et al., 2021a). These maps are also one of the main constraints for state-of-the-art models of stellar wind environments

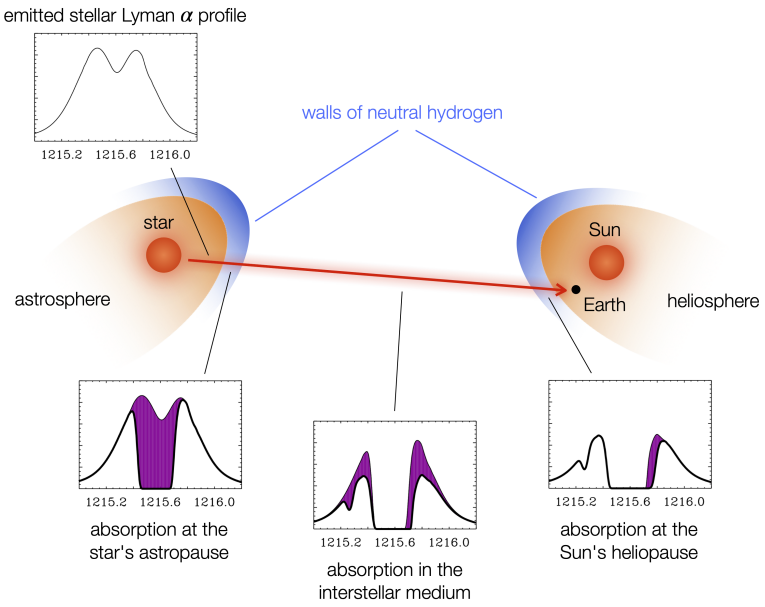

Figure 1.11: Sketch of the formation of the Lyman α absorption profile at 1216 Å initially proposed by Wood et al. (1996). The line profile initially emitted from the star is shown in the top left. Due to the motion of the heliosphere through the interstellar medium, the region where the solar wind plasma dominates, a wall of neutral hydrogen builds up at the heliopause (the edge of the heliosphere). If the star also is a source of a stellar wind, the same process occurs. The wall of neutral hydrogen at the stellar astropause is the first source of absorption of the stellar Lyman α emission as it leaves the system. This is shown in the bottom left panel. The interstellar medium is the next source of absorption (bottom middle panel). Finally, the hydrogen wall at the Sun's heliopause absorbs in the 'red wing' of the line profile (bottom right panel). Depending on the wind mass-loss rate of the star in question, the appearance of the Lyman α at Earth will change. By fitting different models to observed Lyman α, the mass-loss rate of the star can therefore be inferred. Figure adapted from Wood (2004).

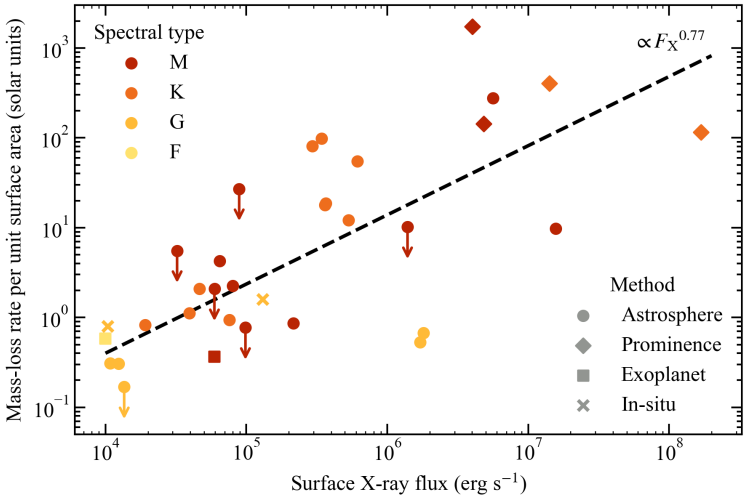

Figure 1.12: Mass-loss rate measurements of all main-sequence low-mass stars obtained to date as a function of their surface X-ray fluxes F_X. The mass-loss rate values ($\dot{M}$) are normalised to the stellar surface area $4\pi {R_\star}^2$, where $R_\star$ is the stellar radius. Each point is coloured by its spectral type, and the symbols illustrate the method used to determine the mass-loss rate. Downward-pointing arrows illustrate where the values are upper-limits. The majority of these are obtained via the fitting of the Lyman α absorption profile of the star as described in the text, which are listed in Wood et al. (2021). The estimates from prominence formation are from Jardine & Collier Cameron (2019), and those from exoplanets are from Kislyakova et al. (2014) and Vidotto & Bourrier (2017). I also show the in-situ measurements of the solar wind. The Sun's X-ray luminosity varies by about an order of magnitude between activity minimum and maximum (Judge et al., 2003), and the mass-loss rate varies from 0.8 to 1.6 times the average value of 1.261×10^{12} g s^{-1} (Finley et al., 2019). The power-law fit to the data from Wood et al. (2021) is shown to illustrate the overall increase in stellar wind mass-loss rate with surface X-ray flux.

for low-mass stars (Chapters 2, 4, and 5). Therefore, below I opt to use the readily-available Φ_V values as opposed to Φ_I. Note that Φ_V values underestimate stellar surface magnetic fluxes compared to those obtained with the Zeeman broadening method, as the ZDI method cannot capture the small-scale magnetic field structure of stars (Reiners & Basri, 2009). However, the two values are generally correlated with one another (See et al., 2019).

The relation between the mass-loss rate per unit surface area of low-mass stars and surface X-ray fluxes derived empirically by Wood et al. (2021) is:

$$\dot{M}/{R_\star}^2 \propto {F_X}^{0.77} \propto {L_X}^{0.77} {R_\star}^{-1.54}. \tag{1.1}$$

Similar to the Zeeman broadening case shown in Figure 1.9, Vidotto et al. (2014) derived the following relation between the X-ray luminosity and the surface magnetic fluxes Φ_V obtained using the ZDI method for GKM dwarfs:

$$L_X \propto {\Phi_V}^{1.80}. \tag{1.2}$$

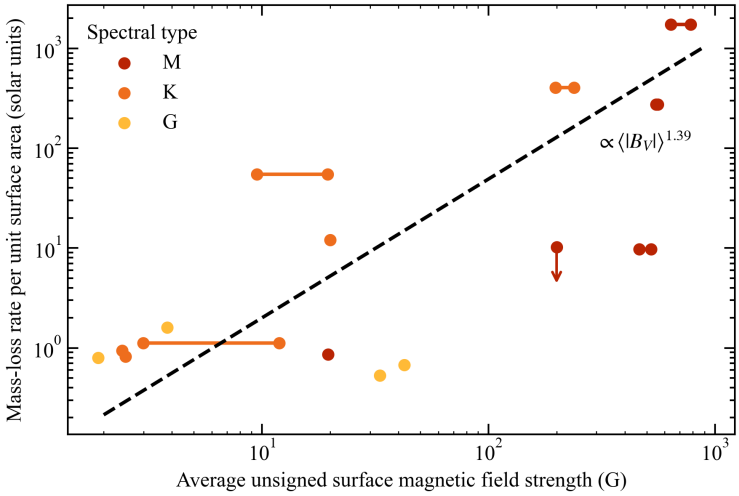

Figure 1.13: Same as Figure 1.12, but for the mass-loss rate per unit surface area as a function of the star's observationally-derived unsigned average surface magnetic field strength $\langle |B_V| \rangle$. For stars with multiple magnetic field maps available, their min/max values of $\langle |B_V| \rangle$ are joined with horizontal lines. The power law derived in Equation 1.3 is overlaid as a dashed line, neglecting the dependence on the stellar radius.

The surface magnetic flux relates to the average unsigned magnetic field strength of the star $\langle |B_V| \rangle$ via $\Phi_V = 4\pi {R_\star}^2 \langle |B_V| \rangle$, giving

$$L_{\rm X} \propto \langle |B_V| \rangle^{1.80} {R_\star}^{3.60}.$$

Combining this with Equation 1.1 then gives

$$\dot{M}/{R_\star}^2 \propto \langle |B_V| \rangle^{1.39} {R_\star}^{1.23}. \tag{1.3}$$

In Figure 1.13, I compare this relation to the observationally-derived values for $\dot{M}/{R_\star}^2$ and $\langle |B_V| \rangle$. These are in good agreement with one another, implying that for low-mass main-sequence stars, stronger magnetic fields drive denser and faster stellar wind outflows. This is neglecting the weaker dependence on the stellar radius in Equation 1.3, which varies from around 0.1 – 1 solar radii for these stars. The values of $\langle |B_V| \rangle$ however span almost three orders of magnitude.

1.5 Star-planet interactions

It was not long after the discovery of the first exoplanet orbiting a main-sequence star in 1995 by Mayor & Queloz (1995) that astronomers began to speculate about interactions occurring between stars and planets. The inspiration for many of these came directly from the theoretical interpretation of observations from RS CVn-type systems. These systems are typically comprised of a main-sequence/subgiant star,

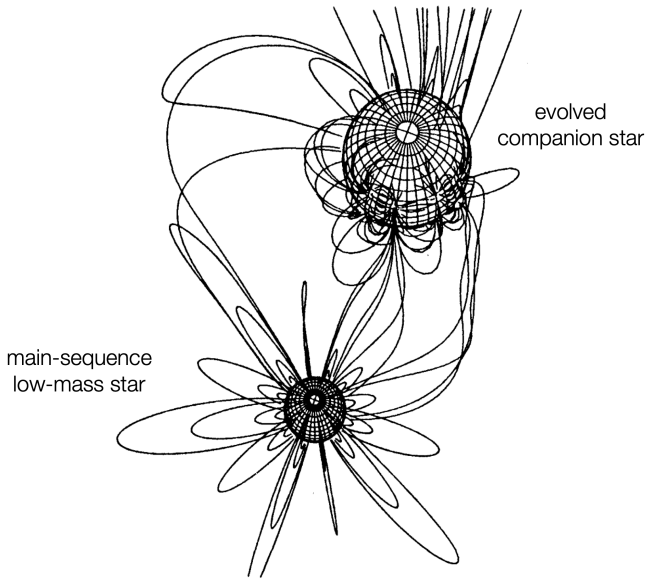

Figure 1.14: Sketch of the magnetic interactions thought to occur in RS CVn binary systems. Reconnection between the magnetic field of the low-mass main-sequence star and the evolved companion star is thought to produce flaring in the system. Although not explicitly shown, tidal interactions between the two bodies are also expected to spin up the main-sequence star, which in turn increases its magnetic activity. In the context of exoplanetary systems, RS CVn systems serve as an analogy for the interactions which may occur between the star and planet. Figure adapted from Uchida & Sakurai (1983).

orbited by a cool, evolved G/K-type companion star (Hall, 1976). The primary star in these systems is thought to be spun-up by the evolved companion star via tidal interactions, enhancing the dynamo of the primary and therefore increasing its activity-related emission compared to if the star was isolated (Drake et al., 1989; Rubenstein & Schaefer, 2000). In addition to this, magnetic interactions between the two stars are also thought to enhance flaring activity, driven by magnetic reconnection. An illustrative sketch is shown in Figure 1.14.

The early population of discovered exoplanets was comprised of Jupiter-sized planets orbiting very close to their stars[2], commonly referred to as 'hot Jupiters'. Soon after their discovery, parallels were made between these hot Jupiter systems and RS CVn binaries. Through similar tidal interactions as in the case of RS CVn systems, hot Jupiters were identified as being sufficient in mass and distance to the star to act as a potential activity enhancer, inducing a tidal bulge on the stellar surface (Cuntz et al., 2000; Saar & Cuntz, 2001). These are often referred to as *tidal* star-planet interactions.

Alongside tidal star-planet interactions, *magnetic* star-planet interactions were also proposed for hot Jupiter systems following from our understanding of RS CVns

[2]NASA Exoplanet Archive

(Rubenstein & Schaefer, 2000; Cuntz et al., 2000; Ip et al., 2004). If like Jupiter these planets have magnetospheres of their own (e.g. Shkolnik et al., 2005; Vidotto et al., 2010; Kislyakova et al., 2014; Cauley et al., 2019), a similar reconnection-driven mechanism could occur between the stellar and planetary magnetic fields, producing enhanced emission on the star. Such a mechanism has been well-studied on Jupiter itself, which interacts *sub-Alfvénically* with its moons Io, Europa, and Ganymede (Neubauer, 1980; Hess et al., 2008; Saur et al., 2013). These interactions produce Alfvén waves, which carry energy back towards Jupiter along the magnetic field line connecting the two bodies, producing prominent emission in the radio via the electron cyclotron maser instability and UV (see Section 1.2; right panel of Figure 1.6; Zarka, 2007; Louis et al., 2017). The criteria for sub-Alfvénic interactions is that the relative velocity between the stellar wind and the planet Δu is less than the Alfvén velocity $u_{\rm A}$, which depends on the plasma density ρ and magnetic field strength B at the planet's position. This is often written as a ratio, which is known as the Alfvénic Mach number:

$$M_{\rm A} = \frac{\Delta u}{u_{\rm A}} = \frac{\Delta u}{B/\sqrt{4\pi\rho}} < 1. \tag{1.4}$$

In the reference frame of the planet, the point where $\Delta u = u_{\rm A}$ is known as the Alfvén surface, which encloses the region where $M_{\rm A} < 1$.

Analogous of the interactions between Jupiter and its moons, sub-Alfvénic interactions have been proposed for exoplanetary systems, with the star and planet taking the roles of Jupiter and the moon respectively (Saur et al., 2013; Turnpenney et al., 2018; Cauley et al., 2019). The criteria for these interactions to occur is that the planet orbits inside the Alfvén surface of the wind of the host star, the magnetic equivalent of the sonic surface. Inside this region, the speed of Alfvén waves exceeds that of the outflowing wind, and the waves can therefore travel back towards the star. The energy they carry is expected to subsequently dissipate near the surface, producing emission at radio (Turnpenney et al., 2018; Kavanagh et al., 2021, 2022), infrared, optical, UV (Shkolnik et al., 2003, 2008; Klein et al., 2022), and X-ray wavelengths (Lanza, 2009; Pillitteri et al., 2011). A sketch outlining this process is shown in Figure 1.15. In late 2021, the first tentative detection of such interactions at radio wavelengths were reported for a sample of main-sequence M dwarfs at radio wavelengths by Callingham et al. (2021).

Another type of interaction thought to occur in exoplanetary systems are those between planets and the winds of their host stars. I will refer to these as *wind-planet* interactions. Signatures of these types of interactions again are predicted to occur across a wide range of wavelengths, and also cover a broad range of different mechanisms. One type of wind-planet interaction is linked to the irradiation of the planet via the star. Close-in exoplanets have been observed to transit their host stars with a much larger effective radius in Lyman α than in the optical (e.g. Lecavelier des Etangs et al., 2012). The theoretical interpretation for this is that the strong stellar X-ray/UV radiation incident on the upper atmosphere of the exoplanet causes it to escape, effectively inflating the planet. This material can readily absorb Lyman α emission, and therefore blocks a much greater fraction of the stellar radiation than in the optical. However, if the wind of the host

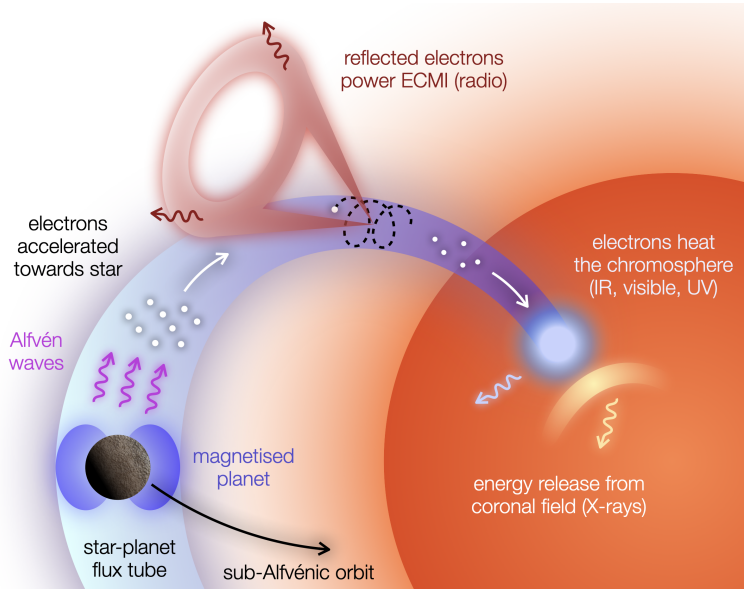

Figure 1.15: Sketch illustrating the different types of radiation associated with magnetic star-planet interactions. Interactions between the planetary and stellar magnetic field produce Alfvén waves, which travel back towards the star. These waves can interact with electrons, accelerating them. Such a process has been identified to power emission via the electron cyclotron maser instability, which produces circularly polarised radio emission. The Alfvén waves can also directly deposit energy at the surface of the star, heating the chromosphere. Signatures of this are thought to occur at infrared, visible, and UV wavelengths. Additional energy may also be released via X-ray emission from the small-scale coronal magnetic field, as suggested by Lanza (2009). Figure from Kavanagh et al. (in prep.).

star is also strong, it may hinder or 'confine' the escape of the irradiated upper planetary atmosphere (Vidotto & Cleary, 2020), therefore altering the Lyman α transit compared to if there was no stellar wind present (Carolan et al., 2021). In theory, by observing Lyman α transits of exoplanets, the mass-loss rates of the host star's wind can be inferred (Vidotto & Bourrier, 2017).

Additional types of wind-planet interactions can also occur if the planet has an intrinsic magnetic field. For instance, if the stellar wind outflow is super-Alfvénic in the reference frame of the planet, a bow shock will form around the planet (Bagenal, 2013). The build-up of material at the nose of the bow shock is thought to form potentially observable signatures in the UV as the planet transits its host star (Vidotto et al., 2010; Llama et al., 2011).

Over the last 30 years, the most searched for signatures of wind-planet interactions are exoplanetary aurorae. In the solar system, the solar wind interaction with the magnetised planets produces bright aurorae that are particularly prominent at radio and UV wavelengths (as discussed in Section 1.2). Zarka (1998) was the first to suggest that the same process could occur on exoplanets providing they are magnetised, which could in theory be used as an alternative way to find new exoplanets and measure their magnetic field strengths.

The main driver in the search for auroral radio emission from exoplanets is firstly that at low frequencies, Jupiter's auroral emission outshines the Sun by roughly 3 orders of magnitude (Zarka, 2007). If the same scenario holds for exoplanets, there should be no issues with regards to the contrast of their emission relative to their host star, as opposed to at other wavelengths (e.g. UV). The second motivating factor comes from the aforementioned radiometric Bode's law (Figure 1.7). As hot Jupiters lie much closer to their host stars than any planet to the Sun, they are expected to experience much stronger stellar winds (Vidotto et al., 2015; Kavanagh et al., 2019). Assuming that the radiometric Bode's law holds for higher incident wind powers, it tells us that the closer a planet gets to its host star, the higher the radio power of its aurora will be. This is also true for planets with larger magnetospheres, which in turn relates to the planet's magnetic field strength, as they intercept a higher magnetic flux from the wind outflow. With the combination of their close-in nature and their potentially strong magnetic fields (Cauley et al., 2019), hot Jupiters could exhibit intense aurorae at radio wavelengths. While searches have taken place over the last 30 years, the first tentative detection of such emission was only recently presented by Turner et al. (2021), who reported potential auroral-like radio emission originating from the hot Jupiter τ Boo b. The reason for the lack of detections is a main topic of Chapters 2 & 3.

1.6 Thesis outline

Chapter 2: Tuning in to the radio environment of HD189733b

In this chapter of the thesis, I explore scenarios for wind-planet interactions occurring on the well-known hot Jupiter HD189733b. This planet orbits very close to its magnetically-active host star at a distance of 0.03 au (3% of the distance between

the Earth and Sun), and is therefore a strong candidate for auroral radio emission following from Sections 1.2 and 1.5. To investigate this, I perform 3D MHD simulations of the wind of the host star, using the BATS-R-US MHD solver (Powell et al., 1999; Tóth et al., 2012). These models are constrained by the observationally-derived surface magnetic field maps of the star during 3 epochs from Fares et al. (2017), providing snapshots of the stellar wind environment around HD189733b. A polytropic index γ is used to mimic the magnetic heating of the corona, wherein the thermal pressure p relates to the density ρ as $p \propto \rho^{\gamma}$.

One of the key findings of this work is that while auroral radio emission could be generated on HD189733b within the detection limits of current-generation radio telescopes such as LOFAR, it may be absorbed significantly by the wind of the star through thermal processes. I refer to these regions as the 'radio photosphere' of the stellar wind, and show that the detection of planetary radio emission is most favourable when the planet is near primary transit, which is very useful for guiding future radio observations. The contents of this chapter were published in the Monthly Notices of the Royal Astronomical Society (MNRAS), 2019, 485, 4529 (Kavanagh et al., 2019).

Chapter 3: Radio eclipses of exoplanets by the winds of their host stars

Following from the results presented in Chapter 2, in this chapter I investigate the effects of different stellar wind properties on the duration where the planet orbits inside the radio photosphere. The morphology of this phenomenon resembles that of an eclipse, and so I refer to it as a 'radio eclipses'. Using a code developed to solve for the wind solution obtained by Parker (1958), I perform a parametric study where I vary the stellar wind temperature and mass-loss rate, as well as the orbital distance and inclination, determining how each affects the duration of the radio eclipses. I show that observing such an eclipse in the radio can be used to infer the properties of the stellar wind, which so far has been limited to a handful of cases (e.g. Figure 1.12). This work was published in MNRAS, 2020, 493, 1492 (Kavanagh & Vidotto, 2020).

Chapter 4: Planet-induced radio emission from the coronae of M dwarfs

The topic of the next chapter shifts towards magnetic star-planet interactions on low-mass stars. The inspiration for this work comes from the recent detections of radio emission from a sample of M dwarfs, some of which are indicative of these types of interactions (i.e. Vedantham et al., 2020; Pérez-Torres et al., 2021; Callingham et al., 2021). In this work, I explore the scenario for magnetic star-planet interactions occurring on the nearby M dwarfs Proxima Centauri (Prox Cen) and AU Microscopii (AU Mic). Both of these stars are host to close-in planets, and have recently had their surface magnetic fields reconstructed by Klein et al. (2021a) and Klein et al. (2021b) respectively. In a similar manner to Chapter 2 I use these maps as constraints for 3D MHD models of the winds of the stars. Note that in this work, I utilised an Alfvén-driven wind model (AWSoM van der Holst et al., 2014), which heats the corona through the dissipation of Alfvén waves, as

opposed to via as polytropic index as used in Chapter 2. The estimated mass-loss rate for Prox Cen of $\dot{M} < 4 \times 10^{-13}\ M_{\odot}\ \mathrm{yr}^{-1}$ (Wood et al., 2001) provides an additional constraint in this work.

The main condition that determines if magnetic star-planet interactions can occur is if the planet orbits inside the Alfvén surface of the stellar wind (Equation 1.4). Using the model for the stellar wind, I show that Prox Cen b orbits outside this region for its entire orbit. Therefore, it is not expected that such interactions could occur, which is at odds with the tentative detections of such interactions suggested by Pérez-Torres et al. (2021). For AU Mic on the other hand, its mass-loss rate is relatively unconstrained. I show that in the case where it has a low mass-loss rate, both planets b and c orbit inside the Alfvén surface for most of the time. This finding shows that a detection or non-detection of magnetic star-planet interactions can be used to estimate the mass-loss rate of low-mass stars, complementing the results of Chapter 3. The results of this work were published in MNRAS, 2021, 501, 1511 (Kavanagh et al., 2021).

Chapter 5: Radio masers on the active M dwarf WX UMa

The final chapter of the thesis focusses on the active M dwarf WX UMa from the sample published by Callingham et al. (2021), which is one of two stars in the sample with available surface magnetic field maps (the other being AD Leo, Morin et al., 2008b; Lavail et al., 2018). In the case of WX UMa, Callingham et al. (2021) suggested that its observed radio emission is likely to be attributed to cyclotron emission, which is expected from magnetic star-planet interactions (Section 1.5). The interesting aspect about WX UMa is that there has yet to be a planet detected to orbit it, which may be due to the fact that the star is very active (Morin et al., 2010). To explore this scenario, I utilise a magnetic field map of the star obtained by Morin et al. (2010) as a constraint for the stellar wind using the AWSoM model. The mass-loss rate for the star is not known, so I estimate it based on its surface X-ray flux via Equation 1.1, giving around the solar value of $2 \times 10^{-14}\ M_{\odot}\ \mathrm{yr}^{-1}$.

I then approach the question in the opposite way to the case of Prox Cen and AU Mic in Chapter 4, which have well-established planetary orbits and properties, which is: where can a planet be placed around WX UMa such that the emission it induces reproduces the observations? To answer this question, I develop a model which accounts for the stellar magnetic field line that connects to the planet at any given time, which determines if the emission can be seen by an observer. By exploring a parameter space for the orbit and properties of the hypothetical planet, and using a prescription for the power of the emission from Saur et al. (2013), I show that a Neptune-sized exoplanet orbiting the star around every 5 days at a distance of 0.034 au can reproduce the observed radio emission from the star. I also derive magnetic field strengths for the planet of 10 – 100 G. The model developed in this work has fantastic applications to future radio observations for identifying planet candidates around active stars.

In this work, I also explore a scenario for generating circularly polarised emission on WX UMa without needing the presence of a planet. This is inspired by the phenomenon on Jupiter, where its auroral emission is in part attributed to

the so-called 'breakdown of co-rotation' (Cowley & Bunce, 2001), as well as that expected from massive magnetised stars (Linsky et al., 1992; Trigilio et al., 2004; Owocki et al., 2022). This type of emission could also reproduce the observations relatively well, albeit with a different modulation than that induced by an orbiting planet. Therefore, models such as this should be explored in future in conjunction with planet-induced models when interpreting potential planet-induced signals.

1.7 Outlook

In this thesis, I have explored scenarios for wind-planet and magnetic star-planet interactions, utilising state-of-the-art stellar wind simulations, which are constrained by information derived directly from a variety of observations. These models provide snapshots of the wind environments of stars, which provide a wealth of information about the plasma surrounding the planet, which is not generally obtainable via other means. The plasma environment tells us if and when interactions between the star and planet can occur, and if so, their strength and modulation. Thanks to the ever-increasing sensitivity of current-generation telescopes such as LOFAR, low-mass stars are beginning to light up the sky at radio wavelengths, many of which are indicative of star-planet interactions. Therefore, there is a mounting need for sophisticated models to predict and interpret these signals, such as those presented in this thesis.

Looking forward, my aspirations for the work presented here are for it to be used to guide and interpret upcoming radio observations. Combining predictions for planets around stars with traditional methods such as the radial velocity and transit method will hopefully lead to the first confirmed detection of an exoplanet in the radio regime. The model developed in the final chapter also has great potential to be applied not only to other stars, but to magnetised exoplanets and brown dwarfs, which are also expected to exhibit similar emission.

In terms of specific systems, Prox Cen has recently become a target of renewed interest in the context of magnetic star-planet interactions, as a new planet has been found to orbit it (Faria et al., 2022). Unlike planet b, which is likely to orbit entirely outside the Alfvén surface (Chapter 4), this newly-discovered planet d orbits sub-Alfvénically for over 50% of its orbit, wherein it could produce observable signatures on the star via magnetic star-planet interactions (Kavanagh et al., in prep.). The utilisation of the model developed in the final chapter of this thesis can be used to predict the morphology of both the radio signal, as well as in the UV, as has been done in the case of AU Mic (Kavanagh et al., 2021; Klein et al., 2022). By planning future observations of the system guided by the model, Prox Cen could serve as a fantastic test bed for benchmarking these models of magnetic star-planet interactions.

Other targets detected in the LoTSS survey are also worth exploring with the model developed in Chapter 5. One example is the inactive star GJ1151 in the sample from Callingham et al. (2021). Due to its inactivity and slow rotation, it is unlikely that its radio emission could be attributed to an alternative emission mechanism such as those explored for WX UMa. In addition, recent radial velocity

searches hint at the presence of a planet around the star (Mahadevan et al., 2021), in agreement with the suggestions of Vedantham et al. (2020). The current missing piece of this puzzle however is the lack of a surface magnetic field map. With this, the radio emission from the star could be interpreted in the same was as for WX UMa, utilising a stellar wind model for the star.